ADVANCED OPTICAL MATERIALS

www.advopticalmat.de

Efficient Metacoupler for Complex Surface Plasmon Launching

Quan Xu, Xueqian Zhang, Minggui Wei, Guanhua Ren, Yuehong Xu, Yanfeng Li, Huabin Wang, Chunmei Ouyang, Jiaguang Han,* and Weili Zhang**

Surface plasmons (SPs) promise versatile potential applications in many aspects and thus have been a subject of enormous interest. As the most essential functionality, efficient coupling of free-space light into complex SP field is of particular interest in current research. Most existing methods only focus on either efficient coupling or complex SP field generation, which is insufficient to support the ever-increasing demand of practical applications. Herein, it is demonstrated both theoretically and experimentally that a metasurface composed of properly designed C-shaped slit resonators can function as an efficient SP coupler. More importantly, it is shown that the phase and amplitude of the coupled SPs can be simultaneously manipulated, which would offer considerable design flexibilities for complex SP launching. This methodology can provide a wide platform for the design and fabrication of high-performance plasmonic devices in the future, especially large-area ones in practical applications.

1. Introduction

Surface plasmons (SPs), a special form of electromagnetic excitations propagating along a metal/dielectric interface, have been widely exploited in various scientific communities, ranging from physics, chemistry to biology.[1–4] Owing to a confinement of the wave to the surface and an enhancement of the optical field, SPs are very attractive in developing next-generation, ultracompact integrated plasmonic circuitry in which light and electric signals can be transferred and processed simultaneously.[5–7] Controlling the wavefront of SPs, although challenging, is highly required in enabling a variety of functional SP devices.[8] In early studies, much attention has been paid to the control of propagating SPs, where free-space light is first coupled to SPs, and then the wavefront of SPs can be manipulated by diffraction units,[9–11] patterned gratings,[12,13] or transformation optics.[14,15] In order to support the ever-increasing demand in both research and applications of plasmonics, and to bring it to the next level, the exploration for new approaches to steering SPs in the launching process has thus been an intrigued research topic, which could significantly simplify the design and fabrication of most integrated plasmonic devices.

Recently, metasurfaces have emerged as an ideal tool for fine control of SPs through the design of suitable subwavelength meta-atoms and the prescribed arrangement of their spatial distributions.[16,17] In particular, subwavelength metallic slit resonators are among the most commonly used unit elements in designing metasurfaces for SP manipulation. Since the locations and orientations of the slit resonators can be carefully chosen using the iterative algorithm,[18] holographic principle,[19,20] Pancharatnam–Berry (P–B) phase concept,[21–23] or coupled mode theory,[24,25] such metasurfaces have shown excellent flexibilities to steer the wavefront of the coupled SPs. However, due to the dipole response of a single slit resonator, the basic unit elements in these metasurfaces are normally arranged at a distance of about one wavelength, and such a small duty cycle significantly limits the conversion efficiency of SPs. On the other hand, innovative metasurfaces with abrupt phase discontinuities have shown unprecedented capabilities of manipulating electromagnetic waves,[26–28] and thus become the current interest and are being actively explored.[29–31] In particular, it has been demonstrated that the momentum difference between free-space light and SPs can be matched by properly arranging the phase discontinuity gradient.[27,32] In conjunction with reflection-type phase discontinuity units, a series of high-efficiency SP couplers have been reported.[27,33–35] However, the conversion efficiency of such couplers decreases significantly as the excitation range increases.[36] That is because the converted driven surface waves are not an eigen mode of the metasurface, and thus, they experience significant scattering before coupling out of the

Q. Xu, Dr. X. Zhang, M. Wei, G. Ren, Y. Xu, Dr. Y. Li, Dr. C. Ouyang, Prof. J. Han, Prof. W. Zhang
Center for Terahertz Waves and College of Precision Instrument and Optoelectronics Engineering
Tianjin University
Tianjin 300072, China
E-mail: cmouyang@tju.edu.cn; jiaghan@tju.edu.cn

Dr. H. Wang
Chongqing Key Laboratory of Multi-Scale Manufacturing Technology
Chongqing Institute of Green and Intelligent Technology
Chinese Academy of Sciences
Chongqing 400714, China

Prof. W. Zhang
School of Electrical and Computer Engineering
Oklahoma State University
Stillwater, OK 74078, USA
E-mail: weili.zhang@okstate.edu

DOI: 10.1002/adom.201701117

excitation range. In addition, these SP couplers only function as normal SP launchers, in which complex SP launching is not implemented.

In this article, we demonstrate that designer metasurfaces composed of *C*-shaped slit resonators (CRs) offer a powerful solution capable of both efficient coupling and complex launching of SPs. The proposed metasurfaces cannot only match the momentum difference between free-space light and SPs and function as efficient SP metacouplers, but can also support the propagation of the coupled SPs, exhibiting greater effectiveness in the case of a large excitation range. More importantly, by carefully altering the geometrical parameters and the rotation angles of the composing CRs, the phase and amplitude of the coupled SPs can be simultaneously manipulated, which could provide significant flexibility in the design of complex SP launching. As a proof of concept, single- and dual-order SP diffractions are demonstrated both theoretically and experimentally. The proposed methodology illustrates the power of the clever implementation combining phase discontinuity with complex SP launching and it may pave a novel way for developing various SP devices.

2. Results and Discussion

2.1. Sample Design and Phase Discontinuity Concept for SP Coupling

Figure 1a shows the schematic of a single CR with the following geometrical parameters: radius r, width w, open angle α, and orientation angle β. The metallic CR is made of a 200 nm thick aluminum film on a silicon substrate. By altering the geometrical parameters, as illustrated in Figure 1b, the CR can be used to produce a controllable phase retardation in the cross polarization over an entire 2π range. Based on this, a spatial distribution of phase discontinuities at the interface between two media can be constructed freely, where the refraction can be expressed by the following generalized formula[26,28]

$$n_t \sin\theta_t = n_i \sin\theta_i + \frac{1}{k_0}\frac{d\varphi}{dx} \tag{1}$$

where n_i and n_t are the refractive indices of the input and output media, respectively; k_0 is the wavenumber of free-space light; θ_i and θ_t are the angles of the incident and transmitted light, respectively, with respect to the normal direction of the metasurface; $\frac{d\varphi}{dx}$ is the phase discontinuity gradient along the x-direction.

In the case of normal incidence (θ_i is equal to zero), θ_t is fully dependent on n_t and $\frac{d\varphi}{dx}$. Based on Huygens's principle, this phenomenon can be understood by considering each CR as a source of secondary wavelets that spread out in the forward direction. As schematically shown in Figure 1c, the transmitted light at the air side ($n_t = 1$) exhibits anomalous refraction with $\theta_t = \arcsin\left(\frac{1}{k_0}\frac{d\varphi}{dx}\right)$, which has been widely studied previously. Because the electric field is always perpendicular to the propagation direction in the free-space, such anomalous refraction is actually constituted by both E_x and E_z components. And the E_z components increase as the θ_t increases. Then in the specific case where the phase gradient equals the SP wavenumber k_{SP}, namely, $\frac{d\varphi}{dx} = k_{SP}$, as schematically illustrated in Figure 1d.

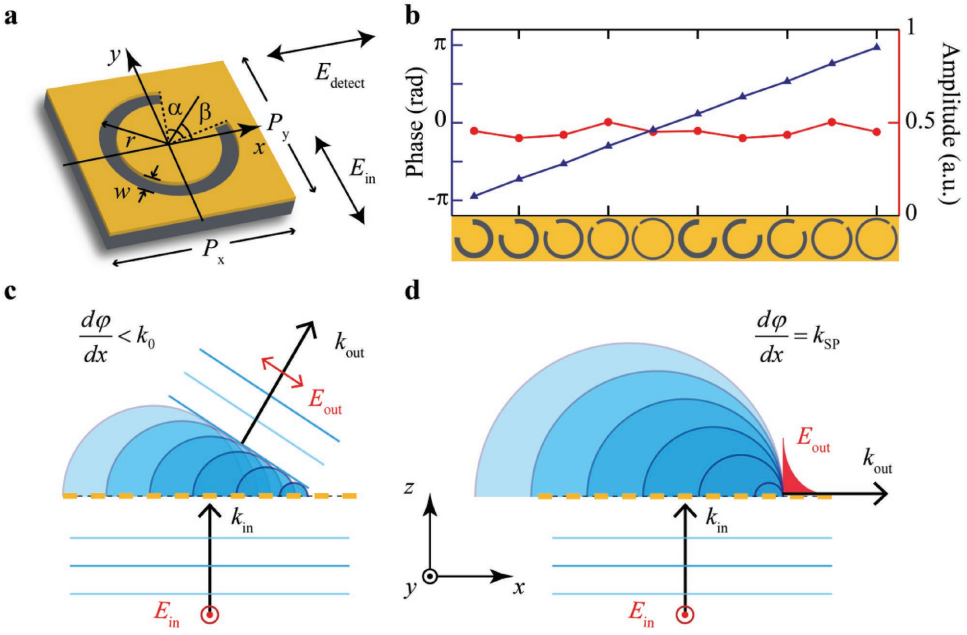

Figure 1. Schematics of *C*-shaped slit resonator (CR) and phase discontinuity concept. a) Schematic view of a single CR, here the $P_x = P_y = 80$ µm. b) Simulated amplitude and phase shift of CRs shown at the bottom at 0.73 THz. Geometrical parameters of former five CRs are $r = 35, 36, 36, 37, 38$ µm, $\alpha = 80°, 65°, 43°, 17°, 10°$, and $w = 10, 9, 7, 6, 5$ µm, respectively, with the same rotation angle $\beta = 135°$. By incorporating the additional *y*-axis-mirrored CRs, a phase shift over an entire 2π range can be achieved. c) and d) Schematics of phase discontinuity concept in the cases of anomalous refraction and SP coupling, respectively.

In this case, the refraction waves are bent to propagate along the surface, where almost all the refraction electric fields exist as E_z components, and thereby be coupled to SPs. As a realistic instance, Section 1 (Supporting Information) illustrates the simulation results of both conditions.

To illustrate the SP coupling behavior of the proposed design scheme, full wave simulations were performed using commercially available software CST Microwave Studio. The super unit is shown as the inset in **Figure 2**a, which is constituted by five CRs with a super period Λ = 400 µm to cover the 2π phase range. Since metals almost behave like perfect conductors in the terahertz regime, the SP dispersion relation is very close to that of the free-space wave, and thus the SPs cannot be confined as well at the metal surfaces as in the visible regime. To increase the confinement, all the metasurfaces are covered with a 20 µm thick dielectric layer (polyimide, $\varepsilon_{\text{polyimide}} = 2.96 + i0.09$).[37] In this case, the $k_{sp} \approx 1.023\ k_0$ at 0.73 THz, which is determined by the eigen-mode solver (see Section 2 in the Supporting Information). A broadband y-polarized plane wave is normally incident from the substrate side to excite the SPs. Figure 2a illustrates the simulated real part of the E_z-field distribution, which is obtained by defining electric field monitors in the xz-plane at $y = 0$ (the center of the CRs), and the metasurface is located at $z = 0$. It can be seen that the excitation exhibits unidirectional launching behavior, and the electric field increases gradually due to the constructive interference caused by the periodic configuration.

2.2. Phase Discontinuity Concept for SP Wavefront Control

So far, we have seen that the SP coupling can be achieved through appropriately designing CRs to satisfy $\frac{d\varphi}{dx} = k_{SP}$. The next problem is how to realize the complex SP launching simultaneously. For a simplified analysis, each row of CRs that satisfy the coupling phase condition $\frac{d\varphi}{dx} = k_{SP}$ can be treated as a source of secondary output SPs. In the case where the phase gradient along the y-direction is zero, namely, a periodic arrangement with $\frac{d\varphi}{dy} = 0$, the output SPs are in phase with each other and collectively produce a normal wavefront, as shown in Figure 2b. Therefore, in order to achieve anomalous SP launching, due consideration must be given to constructing a phase discontinuity gradient of $\frac{d\varphi}{dy}$. As schematically shown in Figure 2c, if we carefully design the phase distribution of each row of the CRs along the x-direction to satisfy $\frac{d\varphi}{dx} = k_{SP}$ and meanwhile tailor each column of CRs along the y-direction with the desired value of $\frac{d\varphi}{dy}$, SP coupling and anomalous SP launching could thus be simultaneously achieved. In addition, if the spatial control of SP amplitude can also be manipulated, more complex SP launching can be achieved.[16,20,23,38,39]

To demonstrate the proposed scheme, three typical samples are numerically designed and experimentally studied here: Sample I—a metasurface for normal SP launching,

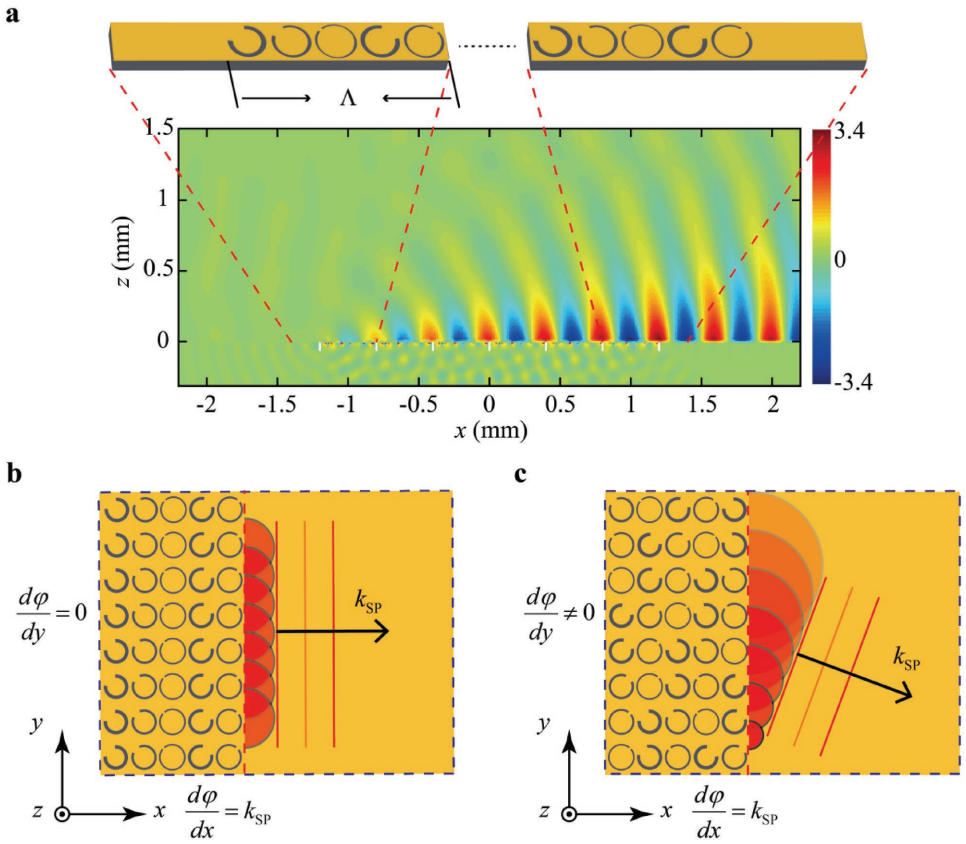

Figure 2. Schematics of super units and SP launching. a) Schematic of CR-based super unit and simulated real part of E_z-field distributions at 0.73 THz. Here six super units along the x-axis are employed. b) and c) Schematics of normal and anomalous SP launching, respectively.

Sample II—a metasurface with a phase gradient $\frac{d\varphi}{dy}$ for anomalous SP launching, and Sample III—a metasurface with the phase gradient $\frac{d\varphi}{dy}$ and also the angular orientation manipulation for amplitude control to achieve complex SP launching. The element resonators in these samples are chosen from the CRs illustrated in Figure 1b according to desired phase (for details see Section 3 in the Supporting Information). All the samples were fabricated using conventional photolithography and metallization processing, and then spin-coated with a 20 µm thick polyimide layer. A near-field scanning terahertz microscopy system (NSTM) was applied to characterize the samples, in which the detector was a near-field photoconductive-antenna-based probe that could measure the SP field by a pair of electrodes sensitive to the E_z component.[40] To allow the detected terahertz pulse to be long enough to cover the entire pulse duration, a 2 mm thick silicon wafer was used as the substrate to avoid Fabry–Perot reflections within 46 ps after the main terahertz pulse.

Figure 3a illustrates the simulated real part of the E_z-field distribution of Sample I, which is obtained in the xy-plane at $z = 50$ µm above the metasurface. The excitation range is marked by a dashed rectangle, and it can be seen that the excited SPs clearly exhibit normal launching wavefront. To experimentally verify the proposed coupling scheme, we fabricated Sample I, in which $\frac{d\varphi}{dx} = k_{SP}$ and $\frac{d\varphi}{dy} = 0$. The corresponding microscopic image is shown in Figure 3b. The coupled SP fields of Sample I were scanned in a range of 1×1.3 mm^2 using NSTM, as shown in Figure 3c, which was started from two wavelengths away from the excitation range, and the probe was placed approximately 50 µm above the sample during scanning, the same as that in the simulation. The measurements clearly show normal SP launching that agrees well with the corresponding simulations and experimentally confirms the proposed coupling scheme. Some of the corresponding time-domain signals are illustrated in the Section 4 (Supporting Information). Furthermore, in order to experimentally compare the coupling efficiency, we also fabricated a metacoupler composed by the most commonly used normal slit resonators, as shown in Figure 3b. The E_z-field amplitudes along the line two wavelengths away from the excitation range (see the white line in Figure 3a) of each metacoupler are scanned and integrated as E^{CR} and E^{Slit}, respectively. Figure 3d illustrates the corresponding measurements, where obviously E^{CR} is much larger than E^{Slit}. The bandwidth of E^{CR} can be calculated as the full width at half maximum $\left(E \geq \frac{\sqrt{2}}{2} E^{CR}_{MAX}\right)$, which equals about 0.07 THz. Notably, because periodic configuration is used in the SP coupler design, the in-plane interference of SPs significantly affects the work bandwidth, where the bandwidth of launched SPs narrows at the frequency that satisfies $\frac{d\varphi}{dx} = k_{SP}$ as the number of period increases. In view of the symmetric excitation feature of normal slit resonators, the coupling efficiency ratio of these two metacouplers can be calculated as $|E^{CR}|^2/2|E^{Slit}|^2 = 4.2$, which experimentally verified the efficient feature of the proposed

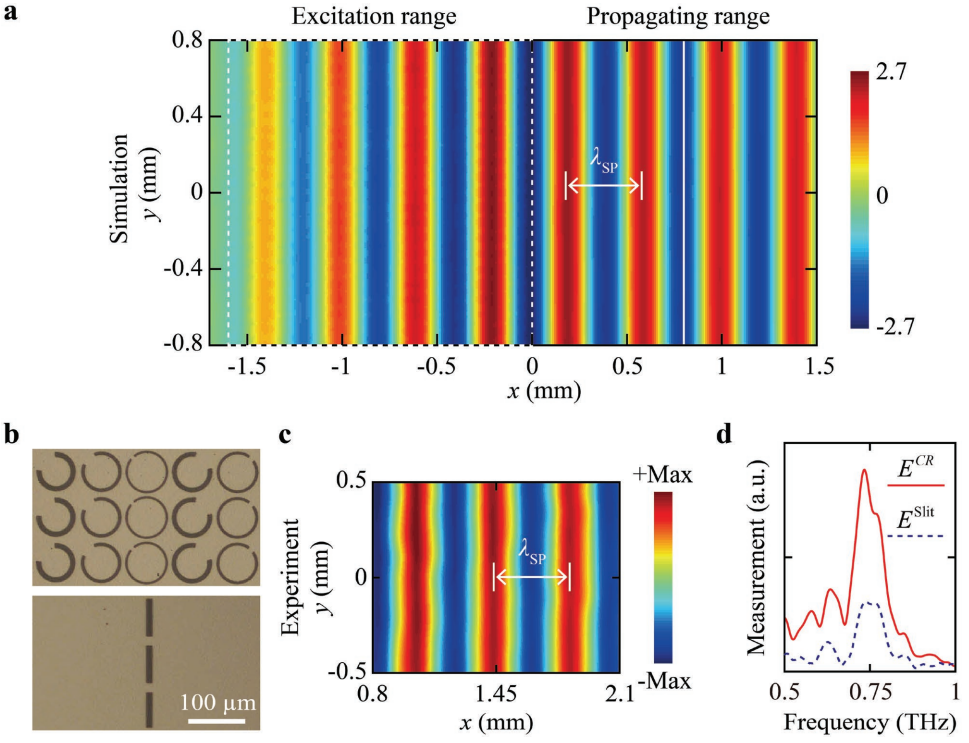

Figure 3. CR-based metasurface for normal SP launching. a) Simulated real part of E_z-field distribution at 0.73 THz. b) Microscopic images of fabricated CR and normal slit resonator samples, respectively. c) Measured real part of E_z-field distributions at 0.73 THz using NSTM. The scan is started at the position about two wavelength away from the excitation range. In this sample, 20 and 60 CRs were used along x- and y-direction, respectively. d) Experimental comparison of SP excitations between CRs and normal slit resonators.

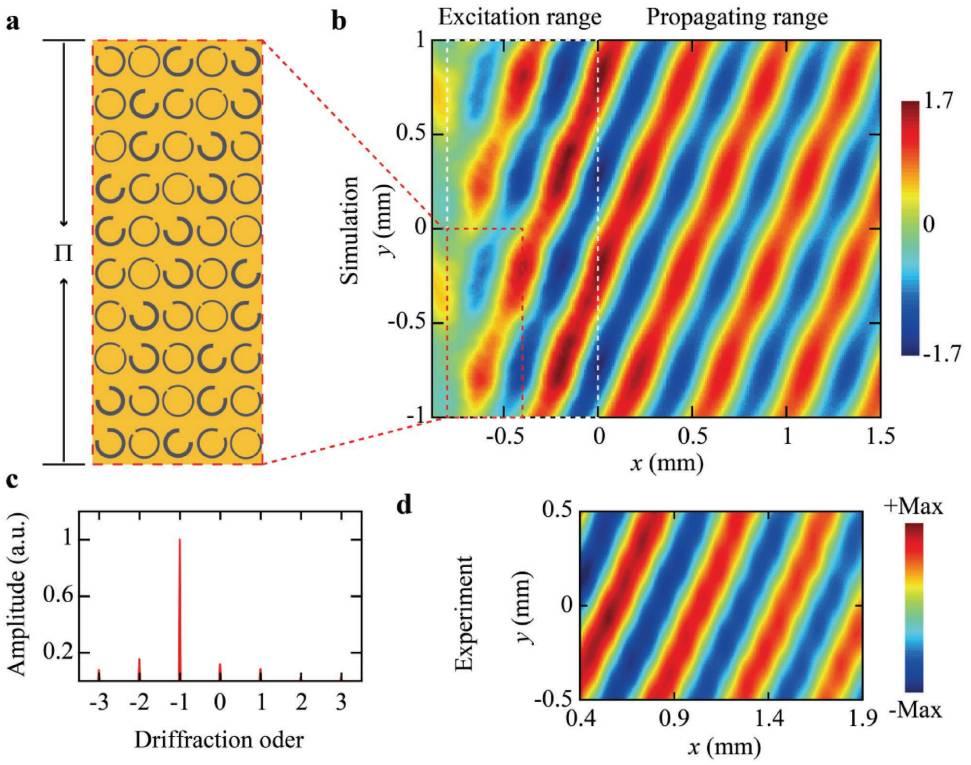

Figure 4. CR-based metacoupler for anomalous SP launching. a) Schematic of metasurface with linear phase gradient along *y*-direction. b) Simulated real part of E_z-field distribution at 0.73 THz. c) and d) Calculated diffraction order distribution from measurements, and measured real part of E_z-field distribution at 0.73 THz using NSTM, respectively. The scan is started at the position about one wavelength away from the excitation range. In this sample, 10 and 60 CRs were used along *x*- and *y*-direction, respectively.

design scheme. However, the conversion efficiency of the proposed coupler cannot be directly measured in the experiments currently. Alternatively, it can be estimated in the simulation by integrating the electric-field intensity over an area above the metal surface, which is approximately 23.3% (see Section 5 in the Supporting Information).

For a demonstration of complex SP launching, we designed Samples II and III to control the diffraction orders of the launched SPs, which functioned as SP gratings. To constitute a grating with desired diffraction orders, the corresponding SP excitation in the *y*-direction can be calculated by[41]

$$E(y) = A(y)e^{i\phi(y)} = \sum_m A_m e^{-i2m\pi y/d} \tag{2}$$

where d is the grating period, m is the diffraction order, and A_m is the amplitude of the m-th diffraction order. In the case of a single diffraction order, $E(y)$ is actually a linear phase profile along the *y*-direction with uniform amplitude, which is also referred to as anomalous SP launching.[22] As a proof of concept, we designed Sample II with $m = -1$ and $d = 1000$ µm, where the composing CRs are schematically illustrated in **Figure 4**a. Here the phase gradient $\frac{d\varphi}{dx} = k_{SP}$ and meanwhile $\frac{d\varphi}{dy} = \frac{2\pi}{\Pi}$ with $\Pi = 1000$ µm. The corresponding simulated real part of the E_z-field distribution in Figure 4b clearly illustrates the anomalous launching of the SPs. In order to experimentally retrieve the information of the diffraction order and verify the anomalous launching performance, we scanned the SP fields of fabricated Sample II using NSTM and then applied Fourier transform to the measured SP fields along the *y*-axis at $x = 1$ mm. The retrieved result is shown in Figure 4c, where a single dominant diffraction order at $m = -1$ can be identified. Furthermore, the measured real part of the E_z-field distribution shown in Figure 4d agrees well with the simulations, experimentally verifying the viability of the anomalous SP launching by the designed phase gradient along the *y*-direction. Such a control scheme is universal, and can be directly applied to other kinds of phase discontinuity concept-based couplers.[27,32–35,42] More importantly, apart from the presented linear phase design, the phase gradient can be encoded with more complicated distributions to achieve functional applications such as SP metalenses or special SP beams.[10,11,22]

In the case of multiple diffraction orders, the amplitude of $E(y)$ is no longer uniform. As an example, **Figure 5**a illustrates the calculated phase and amplitude of $E(y)$ when the diffraction orders are −1st and −3rd where $d = 2000$ µm. To achieve such a grating, obviously amplitude modulation of the excited SPs is desired. Interestingly, it has been proven that when a *C*-ring resonator is rotated, the phase of the scattered light remains the same while the amplitude follows[41]

$$|E| \propto |\sin(2\beta)| \tag{3}$$

where β is the orientation angle. According to the Babinet's principle, this amplitude modulation can also be applied to the CRs. In order to check this modulation for SP coupling, simulation studies were carried out in Section 6 (Supporting

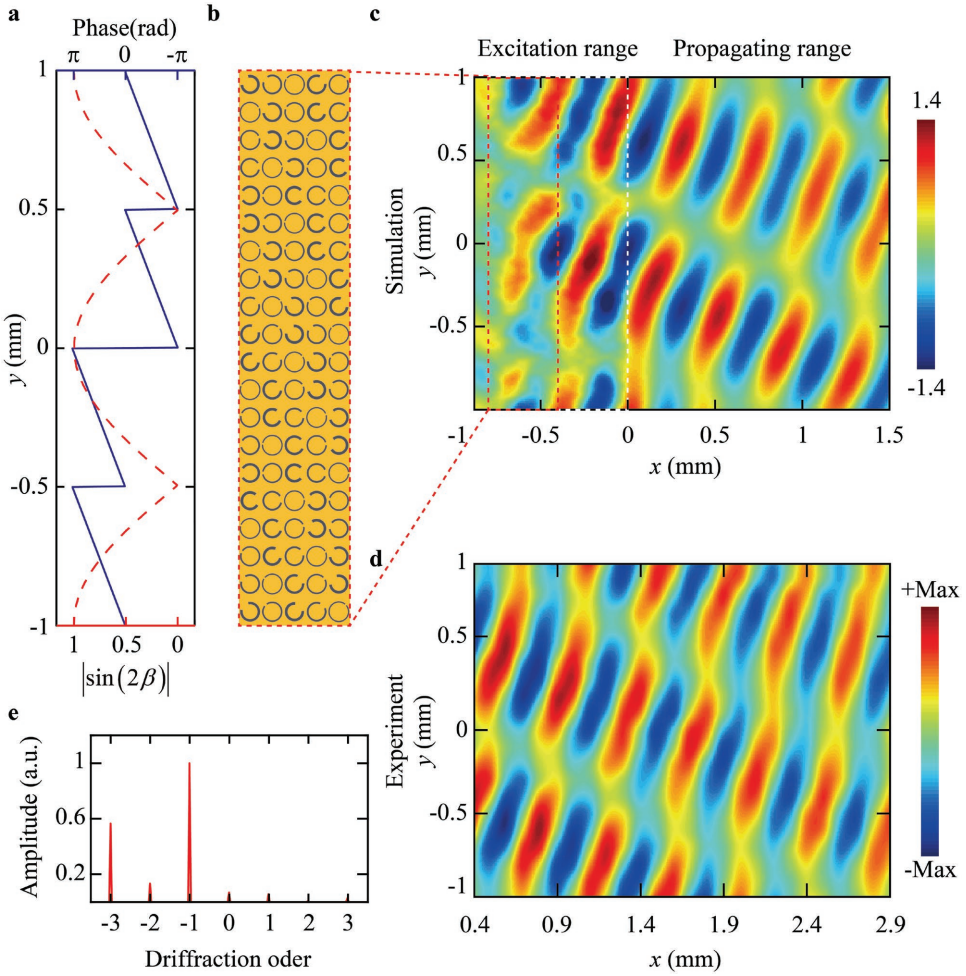

Figure 5. CR-based metacoupler for complex SP launching. a) Desired phase (solid line) and amplitude (dashed line) distributions along *y*-axis to achieve first- and third-order SP diffractions. b) Schematic of metasurface with simultaneous phase and amplitude modulation. c) Simulated real part of E_z-field distribution at 0.73 THz. d,e) Measured real part of E_z-field distribution at 0.73 THz using NSTM, and corresponding diffraction order distribution calculated by Fourier transform, respectively. The scan is started at the position about one wavelength away from the excitation range. In this sample, 10 and 60 CRs were used along *x*- and *y*-direction, respectively.

Information), and the results indicate that the amplitude of SP excitations also follows this rule. Furthermore, we designed Sample III to exploit such a modulation for complex SP launching, as schematically shown in Figure 5b, here the phase gradient along *x*-direction is still $\frac{d\varphi}{dx} = k_{SP}$ and the phase distribution along *y*-direction is correspond to the solid line in Figure 5a. The rotation angle of each CR is calculated by corresponding amplitude (for details see Section 3 in the Supporting Information). The simulated real part of the E_z-field distribution in Figure 5c illustrates clearly the interference between the two diffraction orders. The corresponding measurements are shown in Figure 5d, which agree well with simulations. Furthermore, the calculated diffraction orders from the measurements are shown in Figure 5e, where two dominant diffraction orders at m = −1 and −3 can be observed. These results experimentally confirm the viability of the proposed design scheme. We anticipate such design schemes being used to design more innovative metasurfaces, where the extra design flexibility of simultaneous phase and amplitude control can be used to achieve special SP beaming or holography.[16,20,23,38,39]

2.3. Discussion about the SP Excitation

Conversion efficiency of cross-polarization in single metallic resonance layer has a theoretical limitation of 25%.[43,44] By carefully designing the resonance of realistic structures, this limitation has been experimentally approached in P–B phase metasurface.[45] For manipulating the free-space light by phase discontinuity concept in single metallic resonance layer metasurfaces,[26,28,32] only the cross-polarization can achieve a phase coverage of 2π. Similarly, the CRs also have this limitation. On contrast, manipulating free-space light using reflection-type[27,35] or transmission bilayer and multilayer metasurfaces[46,47] can easily achieve much higher efficiency in either co- or cross-polarizations. By applying the in-plane momentum matching,[27] the metasurfaces mentioned above can all be used

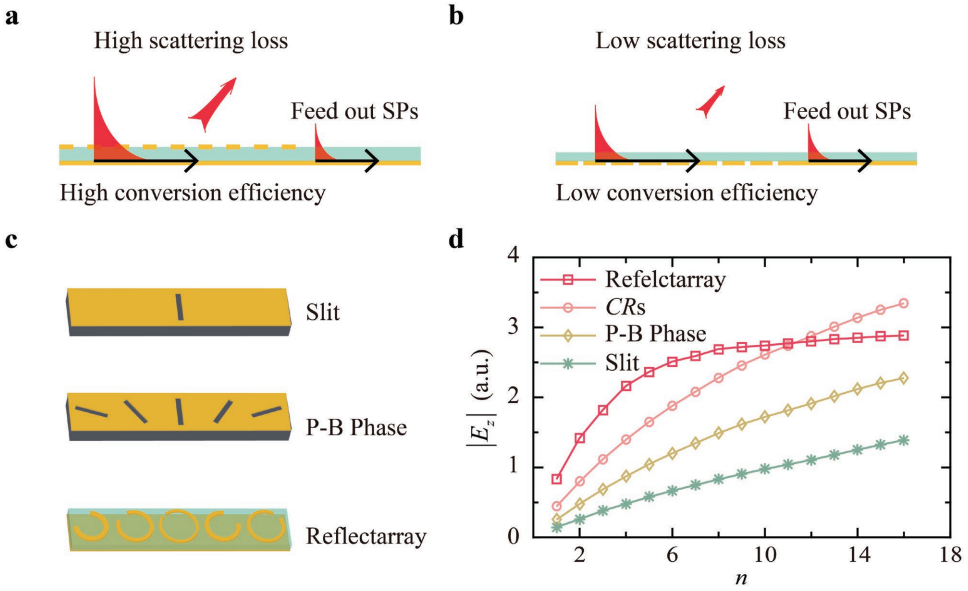

Figure 6. Comparison of different SP excitations. a) and b) Coupling and propagating characters of reflection-type and single-layer SP metacouplers, respectively. c) Schematics of normal slit, P–B phase-based slit array, and reflection-type *C*-ring-based super units, respectively. Here the width and length of slits are 10 and 70 µm, respectively; the orientation angle difference of adjacent slits in P–B phase-based slit array is 36°; the geometrical parameters of *C*-ring resonators are r = 32, 34, 36, 33, 35 µm, α = 95°, 47°, 15°, 70°, 30°, β = 135°, 135°, 135°, 45°, 45°, and w = 9, 7, 5, 8, 6 µm, respectively; the thickness of dielectric spacer is 30 µm. d) Simulated E_z-field amplitudes as a function of super unit number n.

for SP coupler design. And thus the recently reported high-efficiency SP coupler was generally designed using reflection-type metasurfaces.[27,33–35] However, if we take an insight into the SP couplers, we can find that the most important metric is actually the magnitude of the feed-out SPs that could be utilized for the target system. Despite the fact that the reflection-type metacouplers could lead to a high conversion efficiency, they also suffer from significant scattering loss when the generated driven surface waves propagate along the metasurface,[36] as schematically shown in **Figure 6**a. In order to solve this problem, a recently reported work proposed to guide out and support the generated SPs by placing an additional plasmonic layer and experimentally obtained an extremely high efficiency of 73%.[42] However, the strict requirements of the separation and parallel configuration of the SP coupler and plasmonic layer complicate the fabrication, which makes it difficult to extend this scheme to infrared or visible light frequencies. Therefore, more simplified and universal solutions are still required. Then one can consider the single metallic resonance layer metasurfaces, though it has a relatively lower conversion efficiency than that of reflection-type metacouplers, their main body is a metal film that can more favorably support the propagating surface waves, which renders scattering loss lower, as schematically shown in Figure 6b.

To quantitatively analyze the excitation performances, we performed simulations of different kinds of metacouplers, including CRs, P–B phase-based slit array, reflectarray, and also the normal slit resonators. For a fair comparison, the super unit of each coupler has the same period, and the structural parameters of all the basic elements are carefully optimized (corresponding schematics are illustrated in Figure 6c). The SP excitations are obtained by setting the E_z probe to be located two wavelengths away from the excitation range. Figure 6d illustrates the simulated E_z-field-amplitudes as a function of the number of super units n for each metacoupler. Obviously, the SP excitation of the normal slit resonators is much less than that of the others, which can be attributed to a small duty cycle. The recently reported metasurfaces using paired slits with a duty cycle double that of the single slit structure showed an excellent flexibility of SP manipulation, but the SP excitation remained or became even smaller because of the interference between these two slits.[20–23] For the CRs and P–B phase-based slit array, they have a comparable duty cycle and share same efficiency limitation; nevertheless, the SP excitation of the former is higher than that of the latter. That is because the excitations from the B–P phase-based slit array contain both the transverse-magnetic and transverse-electric components, while only the transverse-magnetic-polarized component can be supported for propagation, and therefore, such a mode mismatch reduces the SP excitation.[32,34] In the case of the reflectarray, the SP excitation is initially much larger than that of the other couplers. However, it becomes saturated as n increases due to the large scattering loss, as discussed above. In contrast, the SP excitation growth of the CRs decreases much slower, which causes it to exhibit higher excitation than that of the reflectarray when $n > 11$. A comparison of these excitations indicates that the CR-based metacoupler is not only the most efficient one among the single layer metacouplers, but can also be more efficient even than the reflection-type metacoupler in the case of a large excitation range.

3. Conclusion

Employing CRs as unit elements, we demonstrate an efficient SP metacoupler by cleverly applying the phase discontinuity

concept. Normal SP launching, along with single- and multiple-order SP diffractions, is demonstrated both theoretically and experimentally, reflecting the additional freedom in our design scheme and suggesting further manipulation possibilities. Particularly, the simultaneous phase and amplitude modulation of the coupled SPs have many prospects in practical plasmonic applications and would motivate the design of more complex and innovative metasurfaces. Based on the universal phase discontinuity concept, the proposed design scheme is straightforward and can be applied to a broader electromagnetic spectrum.

4. Experimental Section

Experimental Setup: To characterize the samples, an NSTM system was applied allowing detection of the SP field distribution with a raster scan, which was developed based on traditional terahertz time–domain spectroscopy (THz–TDS). The main difference compared to a regular THz–TDS system was that the terahertz detector in NSTM was replaced with a near-field photoconductive-antenna-based probe.[40] To achieve a movable probe, the detection beam of the system was coupled into a 2 m-length optical fiber. Before coupling into the fiber, a predispersion compensation grating pair was employed to suppress the pulse stretching effect in the fiber. The probe was then fixed onto a 2D electrically controlled translation stage to enable the scanning function.

Sample Fabrication and Characterization: The samples made from a 200 nm thick aluminum film were fabricated on a 2 mm thick silicon substrate by conventional photolithography and metallization process. All the samples were spin coated with a 20 µm thick polyimide layer. To excite SPs, the terahertz beam was incident from the substrate side onto the metallic structures. The incident terahertz beam was collimated with a spot size of 5 mm in diameter, which was large enough to cover the whole excitation area; the linear polarization was achieved using a metallic grid polarizer. During characterization, the detection probe was placed approximately 50 µm above the metasurfaces, the same as in numerical simulations. The scanning resolution for all the samples was 0.1 mm per step, corresponding to about a quarter wavelength of the SP wave. The results shown in Figures 3c, 4d, and 5d are 10 times interpolated from measurements using Matlab.

Supporting Information

Supporting Information is available from the Wiley Online Library or from the author.

Acknowledgements

This work was supported by the National Key Basic Research Program of China (Grant No. 2014CB339800); National Natural Science Foundation of China (NSFC) (Grant Nos. 61422509, 61735012, 61420106006, 61427814, and 61605143); Program for Changjiang Scholars and Innovative Research Team in University (PCSIRT) (Grant No. IRT13033).

Conflict of Interest

The authors declare no conflict of interest.

Keywords

complex launching, metacoupler, metasurfaces, phase discontinuity, surface plasmons

Received: October 19, 2017
Revised: December 17, 2017
Published online: January 19, 2018

[1] W. L. Barnes, A. Dereux, T. W. Ebbesen, *Nature* **2003**, *424*, 824.
[2] J. M. Pitarke, V. M. Silkin, E. V. Chulkov, P. M. Echenique, *Rep. Prog. Phys.* **2007**, *70*, 1.
[3] J. Homola, *Chem. Rev.* **2008**, *108*, 462.
[4] M. L. Juan, M. Righini, R. Quidant, *Nat. Photonics* **2011**, *5*, 349.
[5] T. W. Ebbesen, C. Genet, S. I. Bozhevolnyi, *Phys. Today* **2008**, *61*, 44.
[6] V. J. Sorger, R. F. Oulton, R.-M. Ma, X. Zhang, *MRS Bull.* **2012**, *37*, 728.
[7] Y. Fang, M. Sun, *Light: Sci. Appl.* **2015**, *4*, e294.
[8] I. Epstein, Y. Tsur, A. Arie, *Laser Photonics Rev.* **2016**, *10*, 360.
[9] A. Drezet, D. Koller, A. Hohenau, A. Leitner, F. R. Aussenegg, J. R. Krenn, *Nano Lett.* **2007**, *7*, 1697.
[10] L. Li, T. Li, S. Wang, S. Zhu, X. Zhang, *Nano Lett.* **2011**, *11*, 4357.
[11] L. Li, T. Li, S. M. Wang, S. N. Zhu, *Phys. Rev. Lett.* **2013**, *110*, 046807.
[12] Y. Wang, T. Li, L. Wang, H. He, L. Li, Q. Wang, S. Zhu, *Laser Photonics Rev.* **2014**, *8*, L47.
[13] Y.-G. Chen, Y.-H. Chen, Z.-Y. Li, *Opt. Lett.* **2014**, *39*, 339.
[14] P. A. Huidobro, M. L. Nesterov, L. Martín-Moreno, F. J. García-Vidal, *Nano Lett.* **2010**, *10*, 1985.
[15] T. Zentgraf, Y. Liu, M. H. Mikkelsen, J. Valentine, X. Zhang, *Nat. Nanotechnol.* **2011**, *6*, 151.
[16] I. Epstein, Y. Lilach, A. Arie, *J. Opt. Soc. Am. B* **2014**, *31*, 1642.
[17] C. Zhao, J. Zhang, Y. Liu, *EPJ Appl. Metamater.* **2014**, *1*, 6.
[18] T. Tanemura, K. C. Balram, D.-S. Ly-Gagnon, P. Wahl, J. S. White, M. L. Brongersma, D. A. B. Miller, *Nano Lett.* **2011**, *11*, 2693.
[19] D. Wintz, P. Genevet, A. Ambrosio, A. Woolf, F. Capasso, *Nano Lett.* **2015**, *15*, 3585.
[20] Q. Xu, X. Zhang, Y. Xu, C. Ouyang, Z. Tian, J. Gu, J. Li, S. Zhang, J. Han, W. Zhang, *Laser Photonics Rev.* **2017**, *11*, 1600212.
[21] J. Lin, J. P. B. Mueller, Q. Wang, G. Yuan, N. Antoniou, X.-C. Yuan, F. Capasso, *Science* **2013**, *340*, 331.
[22] X. Zhang, Y. Xu, W. Yue, Z. Tian, J. Gu, Y. Li, R. Singh, S. Zhang, J. Han, W. Zhang, *Adv. Mater.* **2015**, *27*, 7123.
[23] E.-Y. Song, S.-Y. Lee, J. Hong, K. Lee, Y. Lee, G.-Y. Lee, H. Kim, B. Lee, *Laser Photonics Rev.* **2016**, *10*, 299.
[24] X. Zhang, Q. Xu, Q. Li, Y. Xu, J. Gu, Z. Tian, C. Ouyang, Y. Liu, S. Zhang, X. Zhang, J. Han, W. Zhang, *Sci. Adv.* **2016**, *2*, e1501142.
[25] Q. Xu, X. Zhang, Q. Yang, C. Tian, Y. Xu, J. Zhang, H. Zhao, Y. Li, C. Ouyang, Z. Tian, J. Gu, X. Zhang, J. Han, W. Zhang, *Optica* **2017**, *4*, 1044.
[26] N. Yu, P. Genevet, M. A. Kats, F. Aieta, J.-P. Tetienne, F. Capasso, Z. Gaburro, *Science* **2011**, *334*, 333.
[27] S. Sun, Q. He, S. Xiao, Q. Xu, X. Li, L. Zhou, *Nat. Mater.* **2012**, *11*, 426.
[28] X. Zhang, Z. Tian, W. Yue, J. Gu, S. Zhang, J. Han, W. Zhang, *Adv. Mater.* **2013**, *25*, 4567.
[29] H.-T. Chen, A. J. Taylor, N. Yu, *Rep. Prog. Phys.* **2016**, *79*, 076401.
[30] T. J. Cui, S. Liu, L. Zhang, *J. Mater. Chem. C* **2017**, *5*, 3644.
[31] P. Genevet, F. Capasso, F. Aieta, M. Khorasaninejad, R. Devlin, *Optica* **2017**, *4*, 139.
[32] L. Huang, X. Chen, B. Bai, Q. Tan, G. Jin, T. Zentgraf, S. Zhang, *Light: Sci. Appl.* **2013**, *2*, e70.
[33] A. Pors, M. G. Nielsen, T. Bernardin, J.-C. Weeber, S. I. Bozhevolnyi, *Light: Sci. Appl.* **2014**, *3*, e197.

[34] J. Duan, H. Guo, S. Dong, T. Cai, W. Luo, Z. Liang, Q. He, L. Zhou, S. Sun, *Sci. Rep.* **2017**, *7*, 1354.
[35] S. Liu, H. C. Zhang, L. Zhang, Q. L. Yang, Q. Xu, J. Gu, Y. Yang, X. Y. Zhou, J. Han, Q. Chen, W. Zhang, T. J. Cui, *ACS Appl. Mater. Interfaces* **2017**, *9*, 21503.
[36] C. Qu, S. Xiao, S. Sun, Q. He, L. Zhou, *Europhys. Lett.* **2013**, *101*, 54002.
[37] M. Gong, T.-I. Jeon, D. Grischkowsky, *Opt. Express* **2009**, *17*, 17088.
[38] J. Chen, L. Li, T. Li, S. N. Zhu, *Sci. Rep.* **2016**, *6*, 28926.
[39] Y. Tsur, I. Epstein, R. Remez, A. Arie, *ACS Photonics* **2017**, *4*, 1339.
[40] Y. Xu, X. Zhang, Z. Tian, J. Gu, C. Ouyang, Y. Li, J. Han, W. Zhang, *Appl. Phys. Lett.* **2015**, *107*, 021105.
[41] L. Liu, X. Zhang, M. Kenney, X. Su, N. Xu, C. Ouyang, Y. Shi, J. Han, W. Zhang, S. Zhang, *Adv. Mater.* **2014**, *26*, 5031.
[42] W. Sun, Q. He, S. Sun, L. Zhou, *Light: Sci. Appl.* **2016**, *5*, e16003.
[43] F. Monticone, N. M. Estakhri, A. Alù, *Phys. Rev. Lett.* **2013**, *110*, 203903.
[44] A. Arbabi, A. Faraon, *Sci. Rep.* **2017**, *7*, 43722.
[45] X. Ding, F. Monticone, K. Zhang, L. Zhang, D. Gao, S. N. Burokur, A. de Lustrac, Q. Wu, C.-W. Qiu, A. Alù, *Adv. Mater.* **2015**, *27*, 1195.
[46] F. Qin, L. Ding, L. Zhang, F. Monticone, C. C. Chum, J. Deng, S. Mei, Y. Li, J. Teng, M. Hong, S. Zhang, A. Alù, C.-W. Qiu, *Sci. Adv.* **2016**, *2*, e1501168.
[47] Q. Yang, J. Gu, Y. Xu, X. Zhang, Y. Li, C. Ouyang, Z. Tian, J. Han, W. Zhang, *Adv. Opt. Mater.* **2017**, *5*, 1601084.

